Mono- and Dinuclear Ruthenium(II) and Osmium(II) Polypyridine Complexes Built around Spiro-Bridged Bis(phenanthroline) Ligands: Synthesis, Electrochemistry, and Photophysics

Alberto Juris,*,† Luca Prodi,† Anthony Harriman,*,‡ Raymond Ziessel,*,§ Muriel Hissler,§ Abdelkrim El-ghayoury,§ Feiyue Wu,|| Elvira C. Riesgo,|| and Randolph P. Thummel||

Dipartimento di Chimica "G. Ciamician", Università di Bologna, via Selmi 2, 40126 Bologna, Italy, Department of Chemistry, University of Newcastle, Newcastle upon Tyne, NE1 7RU, U.K., Ecole de Chimie, Polymères, Matériaux (ECPM), Laboratoire de Chimie, d'Electronique et de Photonique Moléculaires, associé au CNRS ESA-7008, 25 rue Becquerel, 67087 Strasbourg Cedex 02, France, and Department of Chemistry, University of Houston, Houston, Texas 77204-5641

Received January 5, 2000

Two new dyads have been synthesized in which terminal Ru(II) and Os(II) polypyridine complexes are separated by sterically constrained spiro bridges. The photophysical properties of the corresponding mononuclear complexes indicate the importance of the decay of the lowest-energy triplet states localized on the metallo fragments through the higher-energy metal-centered excited states. This effect is minimized at 77 K, where triplet lifetimes are relatively long, and for the Os(II)-based systems relative to their Ru(II)-based counterparts. Intramolecular triplet energy transfer takes place from the Ru(II)-based fragment to the appended Os(II)-based unit, the rate constant being dependent on the molecular structure and on temperature. In all cases, the experimental rate constant matches surprisingly well with the rate constant calculated for Förster-type dipole−dipole energy transfer. As such, the disparate rates shown by the two compounds can be attributed to stereochemical factors. It is further concluded that the spiro bridging unit does not favor through-bond electron exchange interactions, a situation confirmed by cyclic voltammetry.

Introduction

During the last two decades or so it has become clear that certain Ru(II) and Os(II) polypyridine complexes possess a unique combination of chemical stability, redox behavior, excited-state reactivity, and relatively long-lived luminescence.[1−7] A plethora of such complexes have now been synthesized and studied by means of numerous spectroscopic techniques. Much of this work has been driven by the desire to identify viable sensitizers for the interconversion of light and chemical energy or useful reagents for analytical applications. More recently, attention has focused on polynuclear metal complexes that might exhibit properties different from those of the corresponding monomers, and many such compounds have been prepared and their electrochemical and photophysical properties investigated.[6−8] In particular, special emphasis has been given to the investigation of mixed-metal dinuclear complexes containing both Ru(II) and Os(II) polypyridine units where intramolecular triplet energy transfer takes place.[9−15] An important restriction within this field, however, is the realization that mechanistic details, such as distinguishing between Dexter-type through-bond[16] or Förster-type through-space[17] interactions, can only be attained if the connecting framework is sterically constrained.[8]

Two rigid ditopic ligands, $\mathbf{S^1}$ and $\mathbf{S^2}$, comprising terminal 1,10-phenanthroline chelating units connected via a spiro-based spacer moiety, have been described recently.[18] These ligands retain attractive stereochemical properties with respect to the design of mixed-metal complexes suitable for studying intramolecular triplet energy transfer between the metal centers, and we have now synthesized a range of such materials (Figure 1). Each metallo fragment has the appearance of an $[M(phen)_3]^{2+}$ unit (M = Ru(II) or Os(II); phen = 1,10-phenanthroline) and might be expected to display the well-known electrochemical

† Università di Bologna.
‡ University of Newcastle.
§ CNRS ESA-9008.
|| University of Houston.

(1) De Armond, M. K.; Carlin, C. M. *Coord. Chem. Rev.* **1981**, *36*, 325.
(2) Dodsworth, E. S.; Vlcek, A. A.; Lever, A. B. P. *Inorg. Chem.* **1994**, *33*, 1045.
(3) Meyer, T. J. *Pure Appl. Chem.* **1986**, *58*, 1193.
(4) Juris, A.; Balzani, V.; Barigelletti, F.; Campagna, S.; Belser, P.; von Zelewsky, A. *Coord. Chem. Rev.* **1988**, *84*, 85.
(5) Kalyanasundaram, K. *Photochemistry of Polypyridine and Porphyrin Complexes*; Academic Press: London, 1992.
(6) Scandola, F.; Indelli, M. T.; Chiorboli, C.; Bignozzi, C. A. *Top. Curr. Chem.* **1990**, *158*, 73.
(7) Balzani, V.; Juris, A.; Venturi, M.; Campagna, S.; Serroni, S. *Chem. Rev.* **1996**, *96*, 759.
(8) De Cola, L.; Belser, P. *Coord. Chem. Rev.* **1998**, *177*, 301.
(9) Grosshenny, V.; Harriman, A.; Hissler, M.; Ziessel, R. *J. Chem. Soc., Faraday Trans.* **1996**, *92*, 2223.
(10) Harriman, A.; Romero, F. M.; Ziessel, R.; Benniston, A. C. *J. Phys. Chem. A* **1999**, *103*, 5399.
(11) Collin, J. P.; Gavina, P.; Heitz, V.; Sauvage, J. P. *Eur. J. Inorg. Chem.* **1998**, *1*, 1.
(12) Gulyas, P. T.; Smith, T. A.; Paddon Row: M. N. *J. Chem. Soc., Dalton Trans.* **1999**, 1325.
(13) Chiorboli, C.; Bignozzi, C. A.; Scandola, F.; Ishow, E.; Gourdon, A.; Launay, J. P. *Inorg. Chem.* **1999**, *38*, 2402.
(14) Ward, M. D.; White, C. M.; Barigelletti, F.; Armaroli, N.; Calogero, G.; Flamigni, L. *Coord. Chem. Rev.* **1998**, *171*, 481.
(15) Hage, R.; Lempers, H. E. B.; Hasnoot, J. G.; Reedijk, J.; Weldon, F. M.; Vos, J. G. *Inorg. Chem.* **1997**, *36*, 3139.
(16) Dexter, D. L. *J. Chem. Phys.* **1953**, *21*, 836.
(17) Förster, T. H. *Discuss. Faraday Soc.* **1959**, *27*, 7.
(18) Wu, F.; Riesgo, E. C.; Thummel, R. P.; Juris, A.; Hissler, M.; El-ghayoury, A.; Ziessel, R. *Tetrahedron Lett.* **1999**, *40*, 7311.

10.1021/ic0000202 CCC: $19.00
Published on Web 07/11/2000

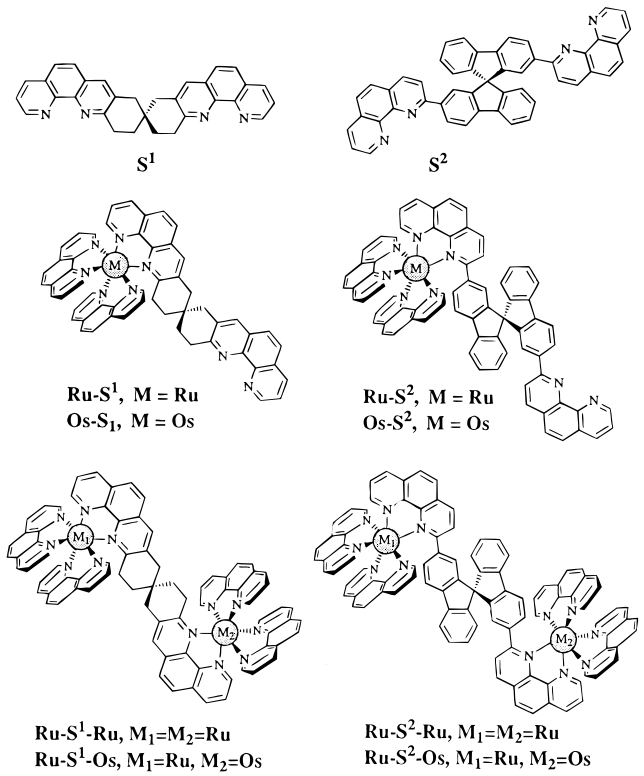

Figure 1. Structures of the ditopic ligands $\mathbf{S^1}$ and $\mathbf{S^2}$ and of the mono- and dinuclear complexes. The counteranions have been omitted for the sake of clarity and should be 2 PF_6^- for the mononuclear and 4 PF_6^- for the related dinuclear complexes.

and photophysical properties of d^6-metal polypyridine complexes. Moreover, in the heterometallic dinuclear species triplet energy transfer is expected to occur from the Ru(II) fragment to the appended Os(II)-based terminal. As such, the rigid nature of the connecting polytopic ligand provides a rare opportunity to explore the mechanism of the energy-transfer step, and it is shown that Förster-type dipole−dipole interactions dominate at both ambient and cryogenic temperatures. This is in contrast to the more common situation where the Dexter mechanism predominates.[19]

Experimental Section

Methods. Infrared spectra were recorded with an IFS 25 Brüker spectrometer with the sample in the form of anhydrous KBr pellets. Fast atomic bombardment (FAB, positive mode) spectra were recorded on a ZAB-HF-VB analytical apparatus in *m*-nitrobenzyl alcohol (*m*-NBA) matrixes using Ar atoms for the bombardment (8 keV). Electrochemical studies were made by cyclic voltammetry with a conventional three-electrode system using a BAS CV-50W voltammetric analyzer. The working electrode was a polished platinum disk while the counter electrode was a platinum wire. A platinum wire was also used as a pseudoreference electrode and was separated from the electroactive solution by a glass frit. Ferrocene was used as internal reference and potentials are quoted versus a saturated calomel electrode (SCE). Reduction potentials were reproducible to within ±20 mV while the reversibility of an individual step was judged by the relative peak currents for forward and reverse steps and from the magnitude of the peak splitting.

Absorption spectra were recorded with either a Shimadzu UV-260, a Perkin-Elmer λ5, or a Perkin-Elmer λ6 spectrophotometer. Molar extinction coefficients are the average of at least two independent measurements and have expected error limits of ±10%. Luminescence studies were made with dilute (ca. 10^{-5} M) acetonitrile solutions at room temperature or in a 4/1 (v/v) methanol/ethanol matrix at 77 K using a Perkin-Elmer LS-50 spectrofluorometer equipped with a red-sensitive Hamamatsu R928 photomultiplier tube. Absorption and emission maxima were reproducible to within ±2 nm. Luminescence spectra were corrected for spectral imperfections by reference to a standard lamp while emission lifetimes were measured with an Edinburgh Instruments model 199 single-photon counting apparatus (D_2 lamp, 310 nm, time resolution 0.5 ns). Luminescence quantum yields were measured with the optically diluted method[20] with reference to $[Ru(bpy)_3]^{2+}$ in air-equilibrated aqueous solution as the quantum yield standard ($\Phi_{LUM} = 0.028$).[21]

Laser flash photolysis studies were made by conventional methods using deoxygenated solutions. Initial studies used a frequency-doubled Nd:YAG laser to deliver single 10-ns pulses to the sample. The monitoring beam was supplied by a pulsed Xe arc lamp, and the signal was detected with a red-sensitive photomultiplier tube after passing through a high radiance monochromator. Differential absorption spectra were recorded point-by-point, after correction for any variation in laser intensity, while kinetic measurements were made at fixed wavelength. Several individual decay records were averaged in order to improve the reliability of the kinetic data. For low-temperature studies, the sample cuvette was housed in an Oxford Instruments optical dewar and cooled to 77 K. Luminescence lifetimes were reproducible to within ±10%.

Improved time resolution was achieved using a frequency-doubled, mode-locked Nd:YAG laser as excitation source. In most experiments, the excitation pulse was Raman shifted to 440 nm using perdeuterated cyclohexane as scattering medium and with a 532-nm notch filter to remove unrequired laser output. Residual laser light was used to generate a white light continuum for use as the monitoring beam, and the two pulses were passed almost collinearly through the sample cell. For spectral studies, the excitation beam was delayed with respect to the monitoring beam using a motorized optical delay line. The monitoring beam was split before the sample cell so as to provide a reference beam, and the two beams were collected after the sample cell with short optical fibers and passed to a Spex spectrograph attached to a Princeton image-intensefied dual-diode array. Approximately 300 individual laser shots were averaged at each time delay. The signals were stored and analyzed in a dedicated PC. Most of the kinetic studies were made with a fast response (rise time 0.9 ns) photodiode detector equipped with a high radiance monochromator tuned to the appropriate wavelength. Again, about 300 individual laser shots were averaged at each wavelength. For high-resolution studies, a double monochromator system was employed. Errors on the various excited-state lifetimes recorded by transient absorption spectroscopy are quoted in the text.

Computer modeling of the average conformation was made by conventional methods using UNIX-based proprietary software run on an SGI workstation. Preliminary structures for the bridging ligands were built using the MacroModel software with the MM2 force field. A full geometry optimization was made for each ligand. The solvent molecules were represented explicitly using the OPLS model and allowing for a cubic box ca. 60 × 50 × 50 $Å^3$ containing about 1600 acetonitrile molecules. The final structure obtained for the bridging ligand was subsequently used to calculate average conformations for the metal complexes. These calculations were made for the dinuclear Ru(II) complexes, with the assumption being made that the corresponding mixed-metal Ru−Os complexes would display identical structures. To maintain neutrality, two perchlorate anions were added for each metal center. The Ru−N distances were kept at 2.06 Å, and the Ru−N angles were maintained at 90° throughout the calculation. Preliminary structures for the dinuclear metal complexes were obtained with the TITAN software package using the SYBYL molecular mechanics force field. Initially, the conformation of the bridging ligand was frozen, but once reasonable structures were obtained, the structure of the entire molecule was subjected to energy minimization. After full energy minimization, refinement was made using PM3 semiempirical molecular orbital parameters. Again, solvent molecules were represented by the OPLS model.

(19) Ziessel, R. *J. Chem. Educ*. **1997**, *74*, 673. Ziessel, R. Hissler, M.; El-ghayoury, A.; Harriman, A. *Coord. Chem. Rev*. **1998**, *178−180*, 1251 and references therein.

(20) Demas, J. N.; Crosby, G. A. *J. Phys. Chem*. **1971**, *75*, 991.

For the Förster calculations, overlap integrals were computed from normalized absorption and emission spectra after full correction for instrumental response and/or baseline drift and transformation into wavenumber. The emission spectra[22,23] were reduced and displayed in the form $(L(\nu)/\nu^3)$ vs ν, where $L(\nu)$ refers to the luminescence intensity at wavenumber ν. Orientation factors were estimated for each pair of possible transitions on the assumption that transition moments are aligned along the metal−N bonds and that each chromophore contributes 6 equal transitions. This results in a total of 36 possible pairs of transitions, and the orientation factor and center-to-center separation distance was calculated for each pair, the separation being equated to the distance between the centers of the metal−N bonds on donor and acceptor. A separate rate constant was established for each pair of transitions, using the MM2 averaged structures, and the overall rate constant was obtained by summing all 36 rates on the basis that the orientation factor can be divided into 36 equal contributions. This approach, which seems superior to simply assuming random orientations and using the metal−metal separation distance, assumes that the promoted electron migrates between the three coordinated polypyridine ligands associated with each chromophore.[24]

Materials. Reagent grade solvents and chemicals were used in the synthesis of the various metal complexes. Chromatographic separations were carried out using neutral aluminum oxide 90, 70−230 mesh (Aldrich). *cis*-$[Ru(phen)_2Cl_2]\cdot 2H_2O$[25] and *cis*-$[Os(phen)_2Cl_2]$[26] were prepared according to literature procedures. Reference compounds were prepared and purified as described earlier,[27,28] while synthetic procedures for the various polytopic ligands have been reported before.[18] Spectroquality solvents were used for photophysical characterization.

Synthesis of the Ruthenium Complexes. To argon-degassed EtOH (50 mL) are added *cis*-$[Ru(phen)_2Cl_2]$ (1 equiv) and the polytopic ligand **S¹** or **S²** (1.1 or 0.55 equiv). After heating of the solution overnight at 90 °C, the solvent was removed under vacuum. The crude product was purified by column chromatography (alumina), eluting with water and acetonitrile using a gradient of water (0−20%). The product was dissolved in the minimum amount of acetonitrile before addition of KPF_6 [10-fold excess in water (10 mL)]. Slow evaporation of the acetonitrile resulted in precipitation of an orange-red solid. This precipitate was washed by centrifugation with water (3 × 10 mL) and diethyl ether (3 × 10 mL). The product was finally purified by passing through a second chromatography column packed with alumina and eluting with CH_2Cl_2/CH_3OH (99/1, v/v).

Ru−S¹: 45% yield; $R_f = 0.59$ (alumina, 95/5 CH_2Cl_2/CH_3OH, v/v). FAB^+-MS (*m*-NBA), *m/e* [M] (% rel int): 1059.3 [M − PF_6] (68); 914.2 [M − $2PF_6$] (100). Anal. Calcd for $C_{55}H_{40}N_8RuP_2F_{12} + CH_3CN$ (M_r = 1203.984 + 41.053): C, 54.99; H, 3.48; N, 10.13. Found: C, 54.75; H,3.26; N, 10.06.

Ru−S²: 95% yield; $R_f = 0.56$ (alumina, 95/5 CH_2Cl_2/CH_3OH, v/v). IR (KBr pellets): ν = 2924 (w), 1627 (m), 1587 (w), 1445 (m), 1427 (m), 1253 (m), 1149 (w), 841 (s) cm^{-1}. FAB^+-MS (*m*-NBA), *m/e* [M] (% rel int): 1134.1 [M − $2PF_6$] (100). Anal. Calcd for $C_{73}H_{44}N_8RuP_2F_{12}$ (M_r = 1424.217): C, 61.56; H, 3.11; N, 7.87. Found: C, 61.42; H, 3.07; N, 7.81.

Ru−S¹−Ru: 70% yield; R_f = 0.30 (alumina, 95/5 CH_2Cl_2/CH_3OH, v/v). IR (KBr pellets): ν = 2910 (w), 1620 (m), 1514 (w), 1239 (m), 1140 (w), 844 (s) cm^{-1}. FAB^+-MS (*m*-NBA), *m/e* [M] (% rel int): 1811.3 [M − PF_6] (100), 1666.2 [M − $2PF_6$] (65). Anal. Calcd for $C_{79}H_{56}N_{12}Ru_2P_4F_{24} + CH_3CN$ (M_r = 1955.404 + 41.053): C, 48.73; H, 2.98; N, 9.12. Found: C, 48.86; H, 3.00; N, 9.50.

Ru−S²−Ru: 52% yield; R_f = 0.42 (alumina, 95/5 CH_2Cl_2/CH_3OH, v/v). IR (KBr pellets): ν = 2910 (w), 1620 (m), 1514 (w), 1239 (m), 1140 (w), 844 (s) cm^{-1}. FAB^+-MS (*m*-NBA): *m/e* [M] (% rel int): 2031.6 [M − PF_6] (6), 1884.9 [M − $2PF_6$] (100), 1740.0 [M − $3PF_6$] (33), 1595.7 [M − $4PF_6$] (13). Anal. Calcd for $C_{97}H_{60}N_{12}Ru_2P_4F_{24}$ (M_r = 2175.637): C, 53.55; H, 2.78; N, 7.73. Found: C, 53.29; H, 2.49; N, 7.53.

Synthesis of the Osmium Complexes. *cis*-$[Os(phen)_2Cl_2]$ (1 equiv) and the polytopic ligand **S¹** or **S²** (1.1 equiv) in degassed EtOH were heated at 90 °C during 1 week. After cooling to room temperature, KPF_6 [10-fold excess in H_2O (10 mL)] was added. Slow evaporation of the organic solvent resulted in precipitation of a brown solid. This precipitate was washed by centrifugation with water (2 × 10 mL) and diethyl ether (3 × 10 mL). The product was finally purified by column chromatography (alumina), eluting with a mixture of CH_2Cl_2/CH_3OH with a gradient of CH_2Cl_2 (0−10%).

Os−S¹: 49% yield; R_f = 0.58 (alumina, 95/5, CH_2Cl_2/CH_3OH, v/v). IR (KBr pellets): ν = 2922 (w), 1627 (m), 1487 (w), 1435 (m), 1205 (w), 1106 (m), 841 (s) cm^{-1}. FAB^+-MS (*m*-NBA), *m/e* [M] (% rel int): 1149.2 [M − PF_6] (100), 1004.2 [M − $2PF_6$] (25). Anal. Calcd for $C_{55}H_{40}N_8OsP_2F_{12} + CH_3CN$ (M_r = 1293.114 + 41.053): C, 51.32; H, 3.25; N, 9.45. Found: C, 51.25; H, 3.12; N, 9.34.

Os−S²: 40% yield; R_f = 0.45 (alumina, 95/5, CH_2Cl_2/CH_3OH, v/v). IR (KBr pellets): ν = 2922 (w), 1627 (m), 1487 (w), 1435 (m), 1205 (w), 1106 (m), 841 (s) cm^{-1}. FAB^+-MS (*m*-NBA), *m/e* [M] (% rel int): 1515.2 [M + H] (4), 1369.2 [M − PF_6] (53), 1224.2 [M − $2PF_6$] (100). Anal. Calcd for $C_{73}H_{44}N_8OsP_2F_{12}$ (M_r = 1513.347): C, 57.94; H, 2.93; N, 7.40. Found: C, 57.62; H, 2.79; N, 7.09.

Synthesis of the Heterodinuclear Complexes. A solution of *cis*-$[Ru(phen)_2Cl_2]$ (1.1 equiv) and $AgBF_4$ (1.5 equiv) in argon-degassed EtOH was heated overnight at 90 °C. After being cooled to room temperature, the deep-red solution was filtered over cotton-wool and quantitatively transferred via cannula to the corresponding **Os−S¹** or **Os−S²** (1 equiv) complex. After the solution was heated 24 h at 100 °C, KPF_6 [10-fold excess in water (10 mL)] was added. Slow evaporation of EtOH led to the precipitation of a brown solid. This precipitate was washed by centrifugation with water (3 × 10 mL) and diethyl ether (3 × 10 mL) and ultimately chromatographed (alumina, 1/5, $MeOH/CH_2Cl_2$, v/v).

Ru−S¹−Os: 55% yield; R_f = 0.26 (alumina, 95/5 CH_2Cl_2/CH_3OH, v/v). IR (KBr pellets): ν = 2926 (m), 2859 (w), 1736 (m), 1631 (m), 1456 (w), 1424 (w), 1292 (w), 1107 (m), 841 (s) cm^{-1}. FAB^+-MS (*m*-NBA), *m/e* [M] (% rel int): 1901.6 [M − PF_6] (100), 1756.6 [M − $2PF_6$] (2), 1611.2 [M − $3PF_6$] (20), 14667 [M − $4PF_6$] (13). Anal. Calcd for $C_{79}H_{56}N_{12}RuOsP_4F_{24} + CH_3CN$ (M_r = 2044.534 + 41.053): C, 46.65; H, 2.85; N, 9.12. Found: C, 46.68; H, 2.84; N, 9.05.

Ru−S²−Os: 85% yield; R_f = 0.26, (alumina, 95/5 CH_2Cl_2/CH_3OH, v/v). IR (KBr pellets): ν = 2926 (m), 2859 (w), 1736 (m), 1631 (m), 1456 (w), 1424 (w), 1292 (w), 1107 (m), 841 (s) cm^{-1}. FAB^+-MS (*m*-NBA), *m/e* [M] (% rel int): 2117.8 [M − PF_6] (34), 1974.9 [M − $2PF_6$] (100), 1829.0 [M − $3PF_6$] (66), 1684.7 [M − $4PF_6$] (13). Anal. Calcd for $C_{97}H_{60}N_{12}RuOsP_4F_{24}$ (M_r = 2264.767): C, 51.44; H, 2.67; N, 7.42. Found: C, 51.18; H, 2.67; N, 7.19.

Results and Discussion

Synthesis. The mononuclear Ru(II) or Os(II) complexes were prepared by selective complexation of one end of the appropriate polytopic ligand with 1 equiv of *cis*-$[Ru(phen)_2Cl_2]\cdot 2H_2O$ or *cis*-$[Os(phen)_2Cl_2]$, while the homodinuclear Ru(II)-based complexes were obtained using a slight excess of the metallo precursor. The heterodinuclear Ru−Os complexes were prepared by metalation of the corresponding monoosmium complexes with 1 equiv of *cis*-$[Ru(phen)_2Cl_2]\cdot 2H_2O$. The alternative

(21) Nakamaru, K. *Bull. Chem. Soc. Jpn.* **1982**, *55*, 2697.
(22) Gould, I. R.; Noukakis, D.; Gomez-Jahn, L.; Young, R. H.; Goodman, J. L.; Farid, S. *Chem. Phys.* **1993**, *176*, 439.
(23) Cortés, J.; Heitele, H.; Jortner, J. *J. Phys. Chem.* **1994**, *98*, 2527.
(24) Using a random orientation and taking an approximate separation distance as the Ru−Os separation would give the following rate constants: **Ru−S²−Os**, $k_{ET} = 5.0 \times 10^7$ at room temperature and $k_{ET} = 4.3 \times 10^6$ s^{-1} at 77 K; **Ru−S¹−Os**, $k_{ET} = 8.9 \times 10^8$ at room temperature and $k_{ET} = 3.6 \times 10^7$ s^{-1} at 77 K.
(25) For dichlorobis(1,10-phenanthroline)ruthenium(II) we used the procedure described for the 2,2′-bipyridine analogue; see: Sullivan, B. P.; Salmon, D. J.; Meyer, T. J. *Inorg. Chem.* **1978**, *17*, 3334.
(26) For dichlorobis(1,10-phenanthroline)osmium(II) we used the procedure described for the 2,2′-bipyridine analogue; see: Kober, E. M.; Caspar, J. V.; Sullivan, B. P.; Meyer, T. J. *Inorg. Chem.* **1988**, *17*, 4587.
(27) For tris(1,10-phenanthroline)ruthenium(II) we used the procedure described for the 2,2′-bipyridine analogue; see: Braddock, J. W.; Meyer, T. J. *J. Am. Chem. Soc.* **1973**, *95*, 3158.
(28) For tris(1,10-phenanthroline)osmium(II) we used the procedure described for the 2,2′-bipyridine analogue; see: Bustall, F. H.; Dwyer, F. P.; Gyarfas, E. C. *J. Chem. Soc.* **1950**, 953.

Table 1. Selected Analytical and Electrochemical Data for the d^6-Complexes Shown in Figure 1

compd	isolated yield %	Anal., %: found (calcd)[a]	FAB$^+$, *m/e* [nature of the cluster][b]	$E_{1/2,\,ox}$, V (ΔE_p, mV; *n*)[c]	$E_{1/2,red}$, V (ΔE_p, mV; *n*)[c]
Ru−S^1	45	C, 54.75 (54.99); H, 3.26 (3.48); N, 10.06 (10.13)	914.2 [M − 2PF$_6$]	+1.35 (62; 1e)	−1.29 (60; 1e), −1.43 (60; 1e), −1.80 (irr)
Os−S^1	49	C, 51.25 (51.32); H, 3.12 (3.25); N, 9.34 (9.45)	1149.2 [M − PF$_6$]	+0.86 (60; 1e)	−1.28 (60; 1e), −1.45 (60; 1e), −1.79 (irr)
Ru−S^1−Ru	70	C, 48.86 (48.73); H, 3.00 (2.98); N, 9.50 (9.12)	1811.3 [M − PF$_6$]	+1.37 (62; 2e)	−1.25 (65; 2e), −1.43 (85; 2e), −1.82 (irr)
Ru−S^1−Os	55	C, 48.68 (46.65); H, 2.84 (2.85); N, 9.05 (9.12)	1901.6 [M − PF$_6$]	+0.86 (62; 1e), +1.33 (75; 1e)	−1.28 (94; 2e), −1.47 (96; 2e), −1.85 (irr)
Ru−S^2	95	C, 61.42 (61.56); H, 3.07 (3.11); N, 7.81 (7.87)	1134.1 [M − 2PF$_6$]	+1.28 (97; 1e)	−1.29 (75; 1e), −1.46 (93; 1e), −1.78 (irr)
Os−S^2	40	C, 57.62 (57.94); H, 2.79 (2.93); N, 7.09 (7.40)	1224.2 [M − 2PF$_6$]	+0.87 (78; 1e)	−1.23 (86; 1e), −1.41 (95; 1e), −1.74 (irr)
Ru−S^2−Ru	52	C, 53.29 (53.55); H, 2.49 (2.78); N, 7.53 (7.73)	1884.9 [M − 2PF$_6$]	+1.28 (96; 2e)	−1.27 (75; 2e), −1.48 (70; 2e), −1.79 (irr)
Ru−S^2−Os	85	C, 51.18 (51.44); H, 2.34 (2.67); N, 7.19 (7.42)	1974.9 [M − 2PF$_6$]	+0.89 (70; 1e), +1.32 (75; 1e)	−1.25 (80; 2e), −1.42 (70; 2e), −1.77 (irr)

[a] Calculated with one CH_3CN solvent molecule for complexes of ligand **S^1**. [b] FAB$^+$ using *m*-nitrobenzylalcohol as matrix only the most intense peak is given. [c] Potentials vs SCE, measured for complexes of **S^2** in DMF + $TBAPF_6$ (0.1 M) using ferrocene as internal reference, Fc^+/Fc = +0.45 V, and for complexes of **S^1** in CH_3CN + $TBAPF_6$ (0.1 M), Fc^+/Fc = +0.30 V; *n* is the number of exchanged electrons; for irreversible processes the value refers to the peak potential.

procedure of prior complexation of one side of the ligand with *cis*-$[Ru(phen)_2Cl_2]\cdot 2H_2O$ followed by attachment of the Os(II)-based fragment to the free site gave significantly lower yields and risked introduction of trace amounts of luminescent impurities in the final sample. All complexes were purified as their hexafluorophosphate salts. Analytical data are collected in Table 1 and fully support the assigned structures. In particular, fast-atom bombardment mass spectrometry provides clear indication of the multicharged complexes owing to the presence of several pseudomolecular peaks corresponding to successive loss of PF_6^- anions, while the isotopic pattern provides further confirmation of the assigned structure.

Electrochemistry. The various complexes were examined by cyclic voltammetry in argon-purged *N*,*N*-dimethylformamide or acetonitrile solution at room temperature, and the results are compared to the parent complexes $[Ru(phen)_3]^{2+}$ and $[Os(phen)_3]^{2+}$. The main findings are collected in Table 1 and can be conveniently divided into oxidation and reduction processes. In all cases, oxidation takes place at the metal center while reduction involves addition of an electron to a polypyridine ligand.

It is well-known that Os(II) complexes are easier to oxidize than the corresponding Ru(II) complexes.[5,7,8] For the parent complex $[Os(phen)_3]^{2+}$ one-electron oxidation of the metal center in acetonitrile occurs with a half-wave potential (E_{ox}) of +0.83 V vs SCE.[29] Similar oxidative processes are seen in the various mono- and bimetallic Os(II)-containing complexes, and there are no significant variations in the derived E_{ox} values. Similarly, one-electron oxidation of $[Ru(phen)_3]^{2+}$ occurs with an E_{ox} of ca. +1.3 V vs SCE[4] while the various mono- and bimetallic Ru(II) complexes exhibit E_{ox} values within the range +1.28 and +1.37 V vs SCE. In the two dinuclear Ru complexes oxidation occurs in a two-electron process due to simultaneous one-electron oxidation of the two Ru moieties. Thus, the spiro unit has little, if any, influence on the redox properties of the terminal metal centers.

Electroreduction of $[Os(phen)_3]^{2+}$ in *N*,*N*-dimethylformamide takes place by way of three reversible one-electron steps[29] with half-wave potentials (E_{red}) of −1.22, −1.39, and −1.74 V vs SCE. These processes have been attributed to successive one-electron reduction of the coordinated ligands. Similar behavior is found for $[Ru(phen)_3]^{2+}$, and it is notable that the derived E_{red} values are not especially sensitive to the nature of the coordinated metal center. The first two reduction waves associated with the **S^1**- or **S^2**-based complexes retain characteristics similar to those observed for the corresponding parent complexes and can be attributed to reduction of the coordinated 1,10-phenanthroline ligands. The third reduction wave is irreversible and is attributed to electron addition to the chelating units of the polytopic ligand. For the dinuclear complexes, these steps correspond to two-electron reduction processes, corresponding to simultaneous one-electron reduction of two phen ligands coordinated to different metals, indicating that there is little electronic communication between the terminals.

Absorption Spectroscopy. UV−vis absorption data are collected in Table 2 while selected spectra of the ligands and complexes are shown in Figures 2−4. For the metal complexes, absorption features found in the UV region (λ < 350 nm) can be ascribed to (nominally) spin-allowed, ligand-centered (^{1}LC) transitions with the intense peak at 265 nm being associated with the various 1,10-phenanthroline units present in the molecule. Absorption bands seen in the visible region (350−550 nm) correspond to (nominally) spin-allowed, metal-to-ligand charge-transfer (^{1}MLCT) transitions whereas the weak bands stretching toward the far-red region are the corresponding (nominally) spin-forbidden (^{3}MLCT) transitions. In agreement with earlier work, the (nominally) spin-forbidden (^{3}MLCT) transitions associated with the Os(II) fragments are both more intense and red shifted relative to those of the analogous Ru(II) counterparts. Note that the fluorenyl chromophore present in **S^2** is apparent in the region 280−380 nm. For the mixed-metal Ru−Os dyads, the derived molar extinction coefficients (ϵ) and the general spectral profiles are in fair agreement with the sum of the individual spectra. To a first approximation, therefore, spectra recorded for the mixed-metal dinuclear complexes look to be a superposition of spectra recorded for the relevant mononuclear complexes. This implies that the metallo terminals are not in strong electronic communication, a conclusion also reached from the electrochemical data.

Luminescence Properties. Polytopic ligands **S^1** and **S^2** fluoresce in fluid solution at room temperature and also phosphoresce in a rigid matrix at 77 K (Figure 2). These characteristic emission profiles are absent in the metal complexes, and

(29) Matsumura-Inoue, T.; Tominaga-Morimoto, T. *J. Electroanal. Chem.* **1978**, *93*, 127.

Table 2. Spectroscopic and Photophysical Data[a]

compd	absorption at 298 K λ_{max}, nm (ϵ, M^{-1} cm^{-1})	luminescence 298 K[b] λ_{LUM}, nm[c]	τ_{LUM}, ns	Φ_{LUM}	77 K λ_{LUM}, nm[c]	τ_{LUM}, μs
Ru−S¹	444 (14 100) 265 (106 000)	614	3.2	4×10^{-4}	573	10.5
Os−S¹	471 (14 200) 267 (108 000)	732	150	1.3×10^{-2}	693	2.10
Ru−S¹−Ru	444 (24 900) 265 (152 000)	626	3.4	4×10^{-4}	577	10.5
Ru−S¹−Os	438 (24 400) 265 (155 000)	730	175	1.2×10^{-2}	692	2.20
Ru−S²	446 (14 500) 265 (116 000)	615	1.4	1.6×10^{-4}	575	10.9
Os−S²	473 (14 200) 266 (111 000)	734	190	1.7×10^{-2}	692	2.20
Ru−S²−Ru	446 (24 800) 266 (167 000)	632	1.2	3.2×10^{-4}	581	9.65
Ru−S²−Os	445 (25 300) 266 (172 000)	736	175	7.1×10^{-3}	696	1.90
$[Ru(phen)_3]^{2+}$	445 (19 000) 262 (116 000)	600	480	2.9×10^{-2}	569	9.65
$[Os(phen)_3]^{2+}$	476 (17 000) 263 (100 000)	718	220	2.0×10^{-2}	691	2.00

[a] In acetonitrile solution at room temperature and in 4:1 (v/v) methanol/ethanol rigid matrix at 77 K. [b] Deaerated solution. [c] Corrected emission maxima.

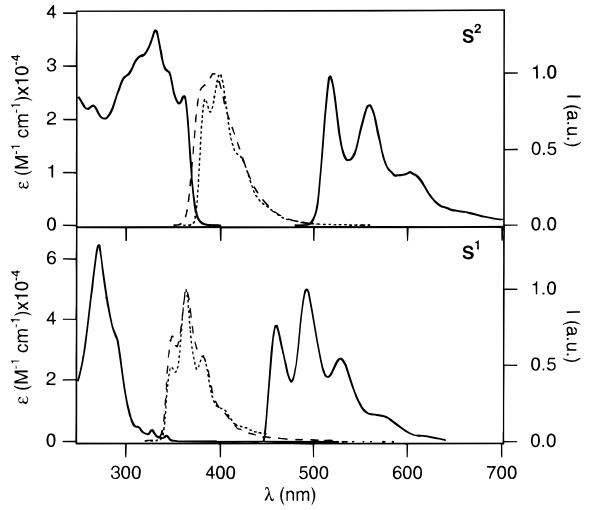

Figure 2. Absorption spectrum (solid line), uncorrected fluorescence spectra at room temperature (dashed line) and at 77 K (dotted line), and phosphorescence spectra (solid line) for the ligands **S¹** and **S²**. Solvents are acetonitrile at room temperature and 4:1 v/v methanol/ethanol at 77 K.

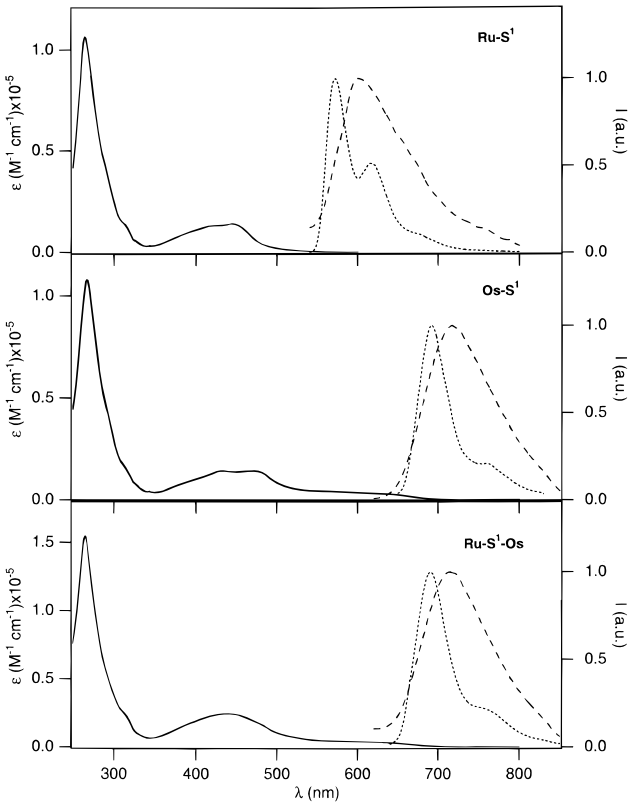

Figure 3. Absorption spectrum (solid line) and uncorrected luminescence spectra at room temperature (dashed line) and at 77 K (dotted line) for **Ru−S¹**, **Os−S¹**, and **Ru−S¹−Os**. Solvents are acetonitrile at room temperature and 4:1 v/v methanol/ethanol at 77 K.

in fact, they are replaced with luminescence spectra that can be attributed to the metal polypyridine fragments[4,5] (Figures 3 and 4). Luminescence maxima (λ_{LUM}), quantum yields (Φ_{LUM}), and lifetimes (τ_{LUM}) measured for the various complexes at ambient and low temperature are collected in Table 2 and are compared to values recorded for the parent complexes $[Ru(phen)_3]^{2+}$ and $[Os(phen)_3]^{2+}$. In each case, the corrected excitation spectrum was in good accord with the absorption spectrum recorded over the entire spectral range. This latter finding suggests that rapid energy transfer occurs from the polytopic ligand to the metal complex, as expected on the basis of the respective energy levels estimated from the emission spectra.

By comparison to $[Ru(phen)_3]^{2+}$ it is apparent that the various mono- and dinuclear Ru(II) polypyridine complexes exhibit typical ^{3}MLCT emission at both 77 and 298 K. The electrochemical results have been interpreted in terms of the most easily reduced ligand being an unsubstituted 1,10-phenanthroline residue, and on this basis, the lowest-energy ^{3}MLCT state should be formed by selective charge injection from metal center to one of these ligands. However, the emission lifetimes and quantum yields recorded at room temperature are significantly decreased relative to the parent compound and this effect is clearly assignable to steric distortion caused by the polytopic ligand. Indeed, there is ample evidence[30−32] to show that substituents at the 2-position of a phenanthroline ligand promote nonradiative deactivation of the ^{3}MLCT state through the upper-lying, metal-centered state. Such interaction is minimized at 77 K, because of the Boltzmann law, but remains important at room temperature. Similar properties are found for the various Os(II)-based complexes, but their lower triplet energies preclude substantial decay through the upper-lying, metal-centered excited state. Consequently, the photophysical properties recorded for the Os(II)-based chromophores are similar to those of the parent complex.

(30) Fabian, R. H.; Klassen, D. M.; Sonntag, R. W. *Inorg. Chem.* **1980**, *19*, 1977.
(31) Deschenaux, R.; Ruch, T.; Deschenaux, P.-F.; Juris, A.; Ziessel, R. *Helv. Chim. Acta* **1995**, *78*, 619.
(32) Araki, K.; Fure, M.; Kishii, N.; Shiraishi, S. *Bull. Chem. Soc. Jpn.* **1992**, *65*, 1220.

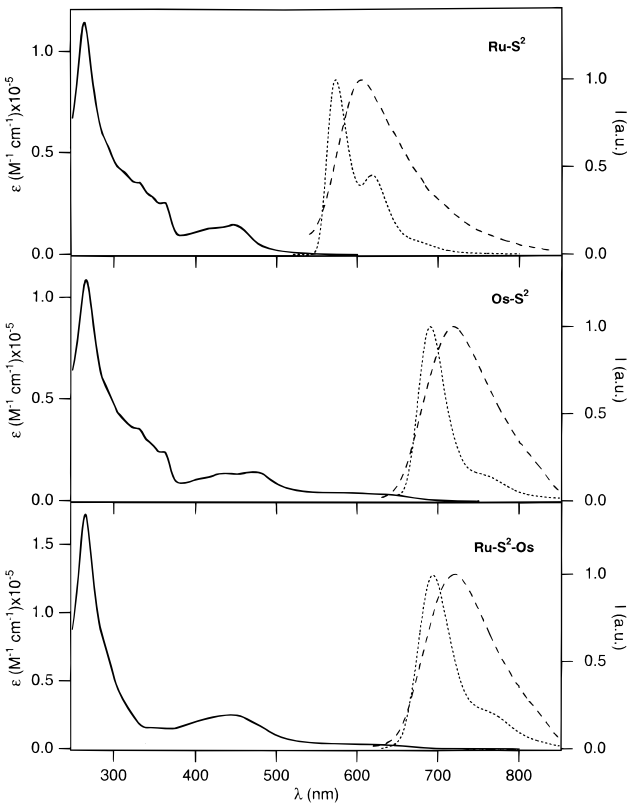

Figure 4. Absorption spectrum (solid line) and uncorrected luminescence spectra at room temperature (dashed line) and at 77 K (dotted line) for **Ru**−**S²**, **Os**−**S²**, and **Ru**−**S²**−**Os**. Solvents are acetonitrile at room temperature and 4:1 v/v methanol/ethanol at 77 K.

At ambient temperature, emission spectra recorded for the two mixed-metal Ru−Os dyads are dominated by luminescence from the Os(II)-based terminals to such an extent that emission from the Ru(II)-based fragments cannot be resolved from the baseline. Although triplet energy transfer might be expected to take place in these systems, the disparate emission quantum yields could easily explain the failure to detect luminescence from the Ru(II)-based terminal. Emission from the Os(II)-based terminal remains comparable to that characterized for the mononuclear complex, and in particular, the emission lifetime remains similar to that of the parent $[Os(phen)_3]^{2+}$. At 77 K, emission probabilities recorded for the Ru(II)- and Os(II)-based reference compounds are comparable and, under such conditions, it should be possible to resolve luminescence from the Ru(II)-based terminal of the mixed-metal Ru−Os dinuclear complexes. This is not the case, however, since the luminescence spectra show only emission from the Os(II)-based fragment, regardless of excitation wavelength. This latter situation is readily accounted for in terms of intramolecular triplet energy transfer along the molecular axis, as observed in many other Ru−Os dyads.[33]

To confirm that triplet energy transfer in the mixed-metal Ru−Os complexes is thermodynamically possible at both temperatures it is necessary to establish triplet energy levels for the individual chromophores. This is easily achieved by curve-fitting analysis of emission spectra recorded for appropriate reference complexes in acetonitrile at room temperature and in an ethanol glass at 77 K. Thus, the corrected emission spectra recorded for the various mononuclear complexes were reduced and normalized before being deconstructed into the minimum number of Gaussian-shaped components of equal half-width.[10] In each case, the entire emission spectrum could be well described in terms of three Gaussian components. The peak of the highest-energy Gaussian component (E_0) can be attributed to the energy difference between 0,0 vibronic levels in the ground and ^{3}MLCT states while the half-width ($\Delta\nu_{1/2}$) can be used to estimate the size of the reorganization energy (λ_T) associated with deactivation of the triplet state.[34]

Table 3. Triplet Lifetimes Recorded for the Reference Compounds by Laser Flash Photolysis in Deoxygenated Acetonitrile at Room Temperature or in an Ethanol Glass at 77 K and the Main Results of a Curve-Fitting Analysis of the Corrected Emission Spectra Recorded under the Same Conditions

compd	temp, K	E_0, cm^{-1}	λ_T, cm^{-1}	E_T, cm^{-1}	$\Delta\nu_{1/2}$, cm^{-1}	τ_T, ns
Ru−**S¹**	298	16 830	1375	18 205	1775	3.2
Ru−**S¹**−**Ru**		16 810	1380	18 190	1780	3.3
Os−**S¹**		14 060	1105	15 165	1590	170
Ru−**S²**		16 800	1380	18 180	1780	1.4
Ru−**S²**−**Ru**		16 840	1360	18 200	1765	1.5
Os−**S²**		14 070	1125	15 195	1605	190
Ru−**S¹**	77	17 530	1325	18 855	885	10 500
Ru−**S¹**−**Ru**		17 550	1310	18 850	880	10 750
Os−**S¹**		14 490	900	15 390	730	2 100
Ru−**S²**		17 500	1325	18 825	885	10 900
Ru−**S²**−**Ru**		17 500	1325	18 825	885	10 600
Os−**S²**		14 490	905	15 395	730	2 200

$$\lambda_T = \frac{(\Delta\nu_{1/2})^2}{16 \ln 2 k_B T} \quad (1)$$

The triplet energy (E_T) can now be expressed as[35]

$$E_T = E_0 + \lambda_T \quad (2)$$

The derived values are collected in Table 3 and clearly indicate that the triplet energy of the Os(II)-based fragment lies well below that of the Ru(II)-based unit, regardless of temperature. The average triplet energy gaps, being ca. 3000 and 3500 cm^{-1}, respectively, at 298 and 77 K, are sufficient to ensure that triplet energy transfer will be unidirectional.

Transient Absorption Spectroscopy. Additional photophysical data were sought from laser flash photolysis studies made at 77 and 298 K. Laser excitation (532 nm, 10 mJ, fwhm = 10 ns) of **Ru**−**S¹**−**Os** and **Ru**−**S²**−**Os** in deoxygenated acetonitrile at room temperature gave rise to transient differential absorption spectra characteristic of the Os(II) fragment without indication of absorption from the Ru(II) unit (Figure 5). Both the metal centers absorb incident photons at 532 nm, but deactivation of the triplet state localized on the Ru(II) unit is complete within the 10-ns laser pulse. Decay of the Os(II)-based triplet occurs via first-order kinetics giving triplet lifetimes (τ_T) of (185 ± 8) and (175 ± 10) ns, respectively, for **Ru**−**S¹**−**Os** and **Ru**−**S²**−

(33) Strouse, G. F.; Worl, L. A.; Younathan J. N.; Meyer, T. J. *J. Am. Chem. Soc.*, **1989**, *111*, 9101. Furue, M.; Yoshidzumi, T.; Kinoshiya, S.; Kushida, T.; Nozakura S.; Kamachi, M. *Bull. Chem. Soc. Jpn.* **1991**, *64*, 1632. De Cola, L.; Barigelletti, F.; Balzani, V.; Belser, P.; Von Zelewsky, A.; Seel, C.; Frank M.; Vögtle, F. *Coord. Chem. Rev.* **1991**, *111*, 255. Vögtle, F.; Frank, M.; Nieger, M.; Belser, P.; Von Zelewsky, A.; Balzani, V.; Barigelletti, F.; De Cola L.; Flamigni, L. *Angew. Chem., Int. Ed. Engl.* **1993**, *32*, 1643. Grosshenny, V.; Harriman A.; Ziessel, R. *Angew. Chem., Int. Ed. Engl.* **1995**, *34*, 1100. Giuffrida, G.; Calogero, G.; Ricevuto V.; Campagna, S. *Inorg. Chem.* **1995**, *34*, 1957. Barigelletti, F.; Flamigni, L.; Guardigli, M.; Juris, A.; Beley, M.; Chodorowski-Kimmes, S.; Collin J. P.; Sauvage, J. P. *Inorg. Chem.* **1996**, *35*, 136.
(34) Murtaza, Z.; Zipp, A. P.; Worl, L. A.; Graff, D. K.; Jones, W. E., Jr.; Bates, W. D.; Meyer, T. J. *J. Am. Chem. Soc.* **1991**, *113*, 5113.
(35) Murtaza, Z.; Graff, D. K.; Zipp, A. P.; Worl, L. A.; Jones, W. E., Jr.; Bates, W. D.; Meyer, T. J. *J. Phys. Chem.* **1994**, *98*, 10504.

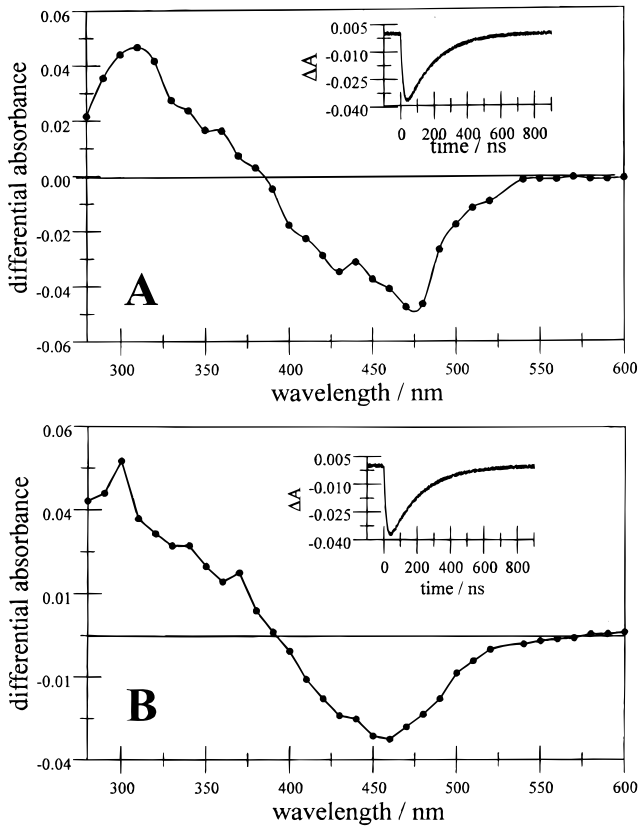

Figure 5. Transient differential absorption spectra recorded 20 ns after pulsed excitation of (a) **Ru**−**S**^{1}−**Os** and (b) **Ru**−**S**^{2}−**Os** in deoxygenated acetonitrile, at 20 °C with a 10-ns laser pulse at 532 nm.

Os. These lifetimes are in good agreement with those derived by luminescence spectroscopy (τ_{LUM}) and remain closely comparable to triplet lifetimes measured for the mononuclear Os(II)-based complexes (Table 2). Separate measurements made with the mono- and dinuclear Ru(II)-based compounds (532 nm, 8 mJ, fwhm = 25 ps) showed that the averaged triplet lifetimes of the Ru(II)-based fragments are 3.5 and 1.2 ns, respectively, for the **S**^{1}- and **S**^{2}-containing complexes (Table 3). As such, it is not surprising that the triplet states localized on the Ru(II)-based fragments have decayed within the 10-ns laser pulse.

The transient differential spectral records collected for the relevant mononuclear complexes indicate that at 385 nm there is an isosbestic point between the ground and ^{3}MLCT excited state of the Os(II)-based unit whereas the ^{3}MLCT of the Ru(II)-based fragment has a positive absorbance at this wavelength. Likewise, at 505 nm the ^{3}MLCT of the Ru(II)-based fragment exhibits an isosbestic point while the ^{3}MLCT excited state of the Os(II)-based unit shows negative absorbance. Such realizations permit selective monitoring of the triplet states localized on Ru(II)- and Os(II)-based fragments, respectively, at 385 and 505 nm for the mixed-metal Ru−Os dinuclear complexes. These experiments require high precision on the wavelength settings and are made possible by the negligible electronic coupling between metal centers in the mixed-metal species.

Under these conditions, it is seen that the ^{3}MLCT of the Ru(II)-based fragment present in **Ru**−**S**^{1}−**Os** decays via first-order kinetics with a lifetime of (560 ± 45) ps (Figure 6a). This decay rate is significantly faster than that found for the reference compounds (Table 3). Furthermore, it is apparent that a substantial fraction of the ^{3}MLCT localized on the Os(II)-based fragment appears after the excitation pulse (Figure 6a). The fast step corresponds to formation of triplet states within the laser pulse and is clearly due to direct absorption of incident photons by the Os(II)-based chromophore. The slower step, which corresponds to a rise time of (490 ± 55) ps, can be attributed to intramolecular triplet energy transfer from the appended Ru(II)-based fragment. For **Ru**−**S**^{2}−**Os**, the ^{3}MLCT of the Ru(II)-based fragment decays with a lifetime of (1.3 ± 0.1) ns, which is very similar to triplet lifetimes recorded for the reference compounds. The ^{3}MLCT localized on the Os(II)-based fragment is formed by direct absorption since there is no clear growth after the excitation pulse (Figure 6b). The indications are, therefore, that intramolecular triplet energy transfer does not take place in **Ru**−**S**^{2}−**Os** at room temperature.

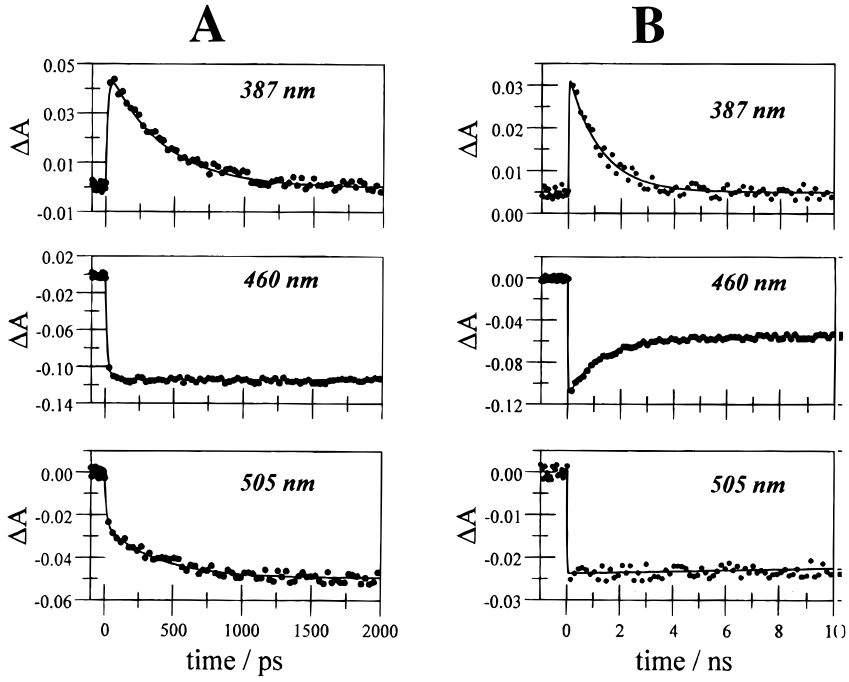

Figure 6. Decay profiles recorded at 387, 460, and 505 nm following pulsed excitation of (a) **Ru**−**S**^{1}−**Os** and (b) **Ru**−**S**^{2}−**Os** in deoxygenated acetonitrile at 25 °C with a 25-ps laser pulse at 440 nm.

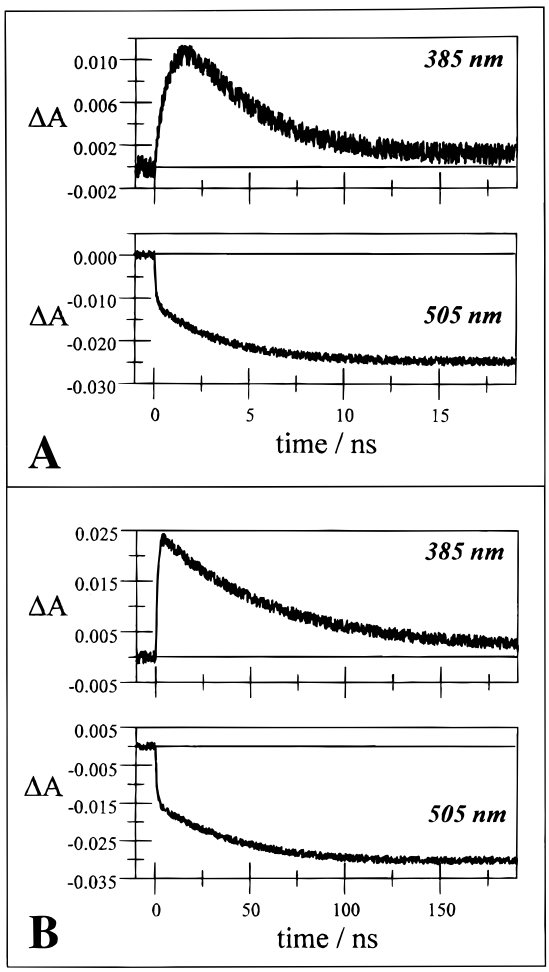

Figure 7. Decay profiles recorded at 385 and 505 nm following pulsed excitation of (a) **Ru−S¹−Os** and (b) **Ru−S²−Os** in deoxygenated ethanol at 77 K with a 25-ps laser pulse at 440 nm.

Identical experiments were made at 77 K using deoxygenated ethanol glasses. Measurements made with the various reference compounds confirmed the triplet lifetimes derived by time-resolved luminescence spectroscopy (Table 2). In particular, it should be noted that, because of decreased mixing with upper-lying metal-centered states, ^{3}MLCT states localized on the Ru(II)-based fragment possess long lifetimes and are more easily able to enter into energy-transfer processes. Under these conditions, the ^{3}MLCT state localized on the Ru(II)-based fragment present in **Ru−S¹−Os** decays via first-order kinetics with a lifetime of (3.6 ± 0.2) ns. This lifetime is ca. 3000-fold shorter than that found for the appropriate reference compounds and indicates that the triplet state is strongly quenched in the mixed-metal complex. Monitoring at 505 nm shows that ca. 50% of the ^{3}MLCT localized on the Os(II)-based unit is formed after the excitation pulse in a unimolecular process for which the lifetime is (3.3 ± 0.7) ns (Figure 7a). Clearly, intramolecular triplet energy transfer along the molecular axis is highly efficient in **Ru−S¹−Os** even at 77 K.

With the heterometallic complex **Ru−S²−Os** in an ethanol glass at 77 K laser flash photolysis studies indicate that the ^{3}MLCT state localized on the Ru(II)-based fragment decays via first-order kinetics with a lifetime of (58 ± 4) ns. Although much longer than found for **Ru−S¹−Os**, this triplet lifetime is still significantly shorter than those recorded for the reference compounds (Table 3). There is a concomitant slow step in the appearance of the ^{3}MLCT state localized on the Os(II)-based fragment, corresponding to a lifetime of (51 ± 6) ns, which is consistent with intramolecular triplet energy transfer (Figure 7b). Consequently, it appears that both mixed-metal Ru−Os complexes support triplet energy transfer at 77 K whereas only **Ru−S¹−Os** demonstrates energy transfer at ambient temperature.

Table 4. Kinetic and Thermodynamic Data Relating to Intramolecular Triplet Energy Transfer in the Mixed-Metal Ru−Os Dyads in Deoxygenated Acetonitrile at Room Temperature and in Ethanol Glass at 77 K

property[a]	Ru−S¹−Os		Ru−S²−Os	
temp, K	298	77	298	77
J_F, 10^{-14} mol^{-1} cm^6	1.84	1.84	1.85	1.88
k_F, 10^7 s^{-1}	173	28	8.4	1.7
τ_T(Ru), ns	0.56	3.6	1.3	58
τ_T(Os), ns	185	2180	175	2200
k_{ET}, 10^7 s^{-1}	147	28	5.5	1.7
ΔE_{TT}, cm^{-1}	3465	3040	2985	3430
λ_{TT}, cm^{-1}	2480	2225	2505	2230

[a] τ_T(Ru) and τ_T(Os) refer respectively to triplet lifetimes measured for the Ru- and Os-based fragments in the mixed-metal complexes; k_{ET} refers to the derived rate constant for intramolecular triplet energy transfer calculated from eq 3; ΔE_{TT} is the energy difference between triplet states localized on Ru- and Os-based fragments; λ_{TT} is the total reorganization energy accompanying triplet energy transfer.

The experimental rate constant (k_{ET}) for intramolecular triplet energy transfer can now be obtained by comparing triplet lifetimes measured for the ^{3}MLCT state localized on the Ru(II)-based fragments present in the mixed-metal (τ_T) and mononuclear (τ_T^0) complexes under identical conditions.

$$k_{ET} = \left(\frac{1}{\tau_T}\right) - \left(\frac{1}{\tau_T^0}\right) \quad (3)$$

The derived values are collected in Table 4. It can be seen that triplet energy transfer is considerably faster for **Ru−S¹−Os** than for **Ru−S²−Os** while there is a 4-fold decrease in rate upon changing from acetonitrile at room temperature to an ethanol glass at 77 K. In both molecular systems, energy transfer is essentially quantitative at 77 K but incomplete at room temperature. It should be noted that the transient absorption spectral records show no obvious indications of light-induced electron transfer while the electrochemical results can be used to show that such processes are unlikely.

Intramolecular Triplet Energy Transfer. There have been many reports of intramolecular triplet energy transfer occurring in mixed-metal Ru−Os complexes, at various temperatures, built around different types of connector. Energy transfer may occur via the Dexter-type electron exchange[16] or the Förster-type Coulombic[17] mechanism, but in most cases it is not possible to resolve the dominant process. Electron exchange is important for flexibly linked systems and in cases where the connector is short and/or conjugated. In contrast, the Coulombic mechanism becomes important when the transition dipoles are well separated or when the connecting organic framework contains saturated units. In fact, the Förster mechanism is promoted by the reasonably high absorption profile in the far-red region of the spectrum associated with the Os(II)-based chromophore since this raises the spectral overlap integral. For the mixed-metal complexes studied here the rigid spiro-type linkage imposes strict stereochemical limits on the average conformation adopted by the molecule and this restriction permits meaningful calculation of the rate constant (k_F) for Förster-type triplet energy transfer.[17]

Thus, k_F can be calculated from the well-known expression (4)

$$k_F = \frac{8.8 \times 10^{-25} K^2 \phi_{LUM} J_F}{n^4 \tau_T R_{CC}{}^6} \quad (4)$$

where Φ_{LUM} and τ_T, respectively, refer to the luminescence quantum yield and triplet lifetime recorded for the mononuclear Ru(II)-based complex under appropriate conditions and n is the refractive index of the solvent at that temperature. The spectral overlap integral (J_F) is readily calculated from normalized absorption and emission spectra, displayed in wavenumbers,

$$J_F = \frac{\int L(\nu)\epsilon(\nu)\nu^{-4}\, d\nu}{\int L(\nu)\, d\nu} \quad (5)$$

Here $L(\nu)$ refers to the corrected luminescence intensity of the donor at wavenumber ν and $\epsilon(\nu)$ is the molar extinction coefficient of the acceptor at that wavenumber. The absorption and emission spectra, respectively, are assumed to refer to the mononuclear Os(II)- and Ru(II)-based complexes. The derived values are listed in Table 4. The final terms required to complete the Förster calculation are the average distance separating the centers of the transition dipoles (R_{CC}) and the orientation factor (K) associated with particular pairs of transition dipoles on donor and acceptor. Using the computer-generated energy-minimized conformation of each mixed-metal dyad, orientation factors and separation distances were calculated for each of the 36 possible pairs of transition dipoles, assuming that each pair contributes equally to the overlap integral. Individual k_F values so obtained were summed to give a global rate constant (Table 4).

It can be seen that the calculated k_F values are in excellent agreement with the experimental rates of intramolecular triplet energy transfer at both 77 and 298 K. At 77 K, where energy transfer is essentially quantitative, the observed and calculated rates are ca. 15-fold higher for **Ru**−**S**$^{\mathbf{1}}$−**Os** than for **Ru**−**S**$^{\mathbf{2}}$−**Os**. This difference can be traced to the shorter separations in the former molecule, where the averaged metal−metal separation is 9.6 Å compared 13.5 Å in **Ru**−**S**$^{\mathbf{2}}$−**Os**. This good agreement between experiment and Förster theory implies that electron exchange is relatively unimportant in these systems, despite the fact that short (i.e., <4 Å) edge-to-edge separations are found for both dyads. This implies that the spiro fragment of the bridging ligand hinders electronic communication between the two metal units, differently from what commonly observed in other dinuclear complexes, where the Dexter mechanism predominates.[8]

Acknowledgment. A.J. and L.P. thank the University of Bologna (Funds for Selected Research Topics) and the MURST (Supramolecular Chemistry Project). R.Z. acknowledges the Centre National de la Recherche Scientifique(CNRS) and the Engineer School of Chemistry in Strasbourg (ECPM) for partial financial support. F.W., E.C.R., and R.P.T. thank the Robert A. Welch Foundation (Grant E-621) and the National Science Foundation (Grant CHE-9714998).

Supporting Information Available: Differential absorbance spectra. This material is available free of charge via the Internet at http://pubs.acs.org.

IC0000202